

1 Article

2 High-Resolution Hologram Calculation method 3 Based on Light Field Image Rendering

4 Xin Yang^{1,2}, FuYang Xu³, HanLe Zhang¹, HongBo Zhang⁴, Kai Huang³, Yong Li^{3,*} and
5 Qiong-Hua Wang^{1,2,*}

6 ¹ School of Instrumentation and Optoelectronic Engineering, Beihang University, Beijing 100191, China;

7 ² Beijing Advanced Innovation Center for Big Data-based Precision Medicine, Beihang University,
8 Beijing 100191, China; holooptics@buaa.edu.cn (X. Y.); hanlezhang@stu.scu.edu.cn (H. Z.)

9 ³ Institute of Information Optics, Zhejiang Normal University, Jinhua, Zhejiang 321004, China; xfy@zjnu.cn
10 (F. X.); 727305480@qq.com (K. H.)

11 ⁴ Department of Computer and Information Sciences, Virginia Military Institute, Lexington 24450, VA, USA;
12 zhangh@vmi.edu (H. Z.)

13 * Correspondence: liyong@zjnu.cn (Y. L.); qionghua@buaa.edu.cn (Q. H. W.)

14

15 **Featured Application:** The proposed method is applicable for static 3D advertising and
16 holographic packaging.

17 **Abstract:** A fast calculation method for the full parallax high-resolution hologram is proposed
18 based on the elemental light field image (EI) rendering. A 3D object located near the
19 holographic plane is firstly rendered as multiple EIs with a pinhole array. Each EI is
20 interpolated and multiplied by a divergent sphere wave and interfered with a reference wave
21 to form a hogel. Parallel acceleration is used to calculate the high-resolution hologram because
22 calculation of each hogel is independent. A high-resolution hologram with four billion pixels
23 is calculated only within 8 minutes. Full parallax high-resolution 3D displays are realized by
24 optical reconstructions.

25 **Keywords:** holographic 3D display; computer generated holography; light field image rendering;
26 pinhole array

27

28 1. Introduction

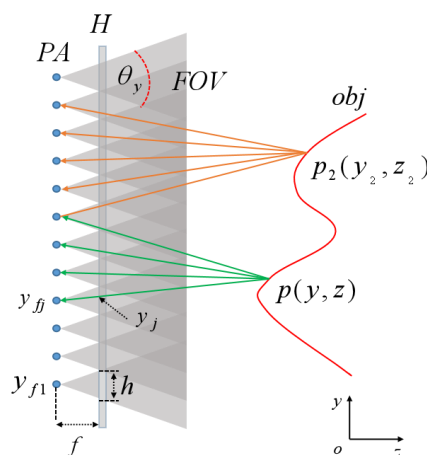
29 Holography can fully reconstruct 3D scene with all phase and amplitude information. The
30 traditional optical holography can record very high-resolution hologram with laser as illumination
31 but stable optical platform is needed as well as other optical devices. Different from the optical
32 holography, the 3D information can be coded into a computer generated hologram for holographic
33 3D display [1,2]. Many efforts for dynamic holographic displays have been made for monochrome
34 display or color display using laser or LED as illumination [3-8]. The progresses on dynamic
35 holographic 3D display, however, still have proven difficult due to the constraints of limited
36 bandwidth of current available spatial light modulator (SLM) and huge amount of calculation.

37 High-resolution holograms such as rainbow holograms and Fresnel holograms are applicable
38 for 3D advertising and packaging because of the emerging of holographic printing technology
39 [9-14]. The biggest challenge for high-resolution holography is the huge amount of computation.
40 Multiple algorithms such as point cloud-based, layer-based, triangular mesh-based algorithms as
41 well as the holographic stereogram methods have been proposed [15-18]. However, those methods
42 are not effective for reducing the calculation burden for high-resolution hologram. We have

43 proposed frequency fusing methods similar to holographic stereogram for full-parallax image
 44 hologram [11] and color rainbow hologram [10] calculation with high efficiency but the sizes of
 45 calculated hologram are limited by the RAM (Random Access Memory) of computer. Rectangular
 46 tiling algorithms have been proposed for high-resolution hologram calculation free of limitation
 47 from computer RAM [19,20]. Taking the reference [19] as an example, each rectangular tile is
 48 calculated by using the 3D object data within the field of view (FOV) of this tile using point
 49 cloud-based method. A full-parallax hologram with a resolution of 20000×20000 can be up to 32.9
 50 hours. Another rectangular tiling based algorithm is integral holography, which is the combination of
 51 integral imaging 3D display and holography [21-24]. In this method, each element light field image
 52 (EI) rendered from micro-lens array or pinhole array is firstly fast Fourier transformed (FFT) as the
 53 complex amplitude of each elemental hologram or called hogel. And then the hogel is calculated by
 54 interference the complex amplitude with a reference wave. However, the calculation of complex
 55 amplitude using FFT is time consuming especially for large scale hologram calculation.

56 In order to reduce the computational time of the high-resolution hologram and inspired from
 57 integral holography, a simple and fast calculation method without using FFT is proposed. A pinhole
 58 array is set behind the holographic plane for rendering EIs. Each EI located on the holographic plane
 59 is multiplied with a divergent spherical wave, which is regarded as the complex amplitude of this
 60 hogel. And a reference wave is interfered with complex amplitude for this hogel calculation. Parallel
 61 acceleration is used to speed up the calculation because the calculation of each hogel is independent.
 62 A full parallax high-resolution hologram with a resolution of $200K \times 200K$ is calculated only within 8
 63 minutes. The validity of this proposed method is approved by optical reconstructions.

64 2. Methods



65

66

Figure 1. The rendering of EIs with a pinhole array for hologram calculation.

67 Figure 1 shows the rendering of EIs with a pinhole array for hologram calculation. PA is a
 68 pinhole array behind the holographic plane H. The distance between PA and H is f . obj is a 3D object
 69 in space and $p(y, z)$ and $p_2(y_2, z_2)$ are two object points of obj. The EI on holographic plane has a
 70 width of h and the FOV is depended on the angle θ_y of the EI to the corresponding pinhole in the y
 71 direction. Each EI is closely adjacent to other EIs. The coordinate of j -th pinhole is y_{jf} and projections
 72 of point $p(y, z)$ and $p_2(y_2, z_2)$ within the FOV to each pinhole are demonstrated. The intersections
 73 of projection lines to each pinhole on holographic plane are coordinates of projected point of EI. Such
 74 as shown in Figure 1, y_{pj} is the coordinate of EI in the y direction, which can be expressed as:

$$y_{pj} = f \frac{y - y_{fj}}{z} + y_{fj}. \quad (1)$$

The calculation can also be applied to the x direction and x_{pi} of projected EI can be expressed as:

$$x_{pi} = f \frac{x - x_{fi}}{z} + x_{fi}, \quad (2)$$

where (x, y, z) is the coordinate of the object point P in 3D coordinate system and (x_{pi}, y_{pj}) is the coordinate of EI $im_{i,j}$ on holographic plane. (x_{fi}, y_{fj}) is the coordinate of the $(i-th, j-th)$ pinhole. The $(i-th, j-th)$ EI can be expressed as:

$$im_{i,j}(x_{pi}, y_{pj}) = A_p, \quad (3)$$

where A_p is the amplitude of object point P, (i, j) is the index of EI. The phase of this EI on holographic plane is

$$phs_{i,j}(x_{pi}, y_{pj}) = \frac{2\pi}{\lambda} [\sqrt{(x_{pi} - x_{fi})^2 + (y_{pj} - y_{fj})^2 + f^2}]. \quad (4)$$

The complex amplitude of object wave-front corresponding to each EI is the multiply of Eq. (3) by a divergent sphere wave with the phase illustrated in Eq. (4). This concept is simple and straightforward. From the view of local area, the local amplitude and spherical wave control the amplitude and propagation direction of this small beamlet.

Assuming that the reference light is a plane wave and the angle between the plane wave in the y direction and the z axis is θ_{refy} . The off-axis amplitude type $(i-th, j-th)$ hogel can be expressed as:

$$H_{i,j}(x_{pi}, y_{pj}) = im_{i,j}(x_{pi}, y_{pj}) \cos[phs_{i,j}(x_{pi}, y_{pj}) - \frac{2\pi}{\lambda} y_{pj} \sin(\theta_{refy})]. \quad (5)$$

3. Experiment and results

The pixel pitch d_h of the hologram is 0.318 μm , which is determined by our holographic printer [9-11]. This principle of the home-made holographic printer is similar with the holographic printer introduced in reference [12], but the light source in our holographic printer is a blue LED with center wavelength of 365 nm rather than a laser. The max frequency that the holographic printer can be supported is $\frac{1}{2d_h} = 1573$ line/mm. Printing holograms at the highest resolution requires extremely stability for the printing system. In the practical usage, almost half of the highest resolution is used for hologram design. In the experiment, the diffraction angles of the FOV in the x and y directions are set as: θ_x is 48° and θ_y is 20° , respectively. And the angle of reference wave in the y direction and z axis is set as 22° . Assuming the wavelength is 632 nm. Therefore, the max frequency is $\frac{\sin(\theta_x/2)}{\lambda} = 643$ line/mm in the x direction and the max frequency is $\frac{\sin(\theta_y/2)}{\lambda} + \frac{\sin(\theta_{refy})}{\lambda} = 867$ line/mm in the y direction, respectively. Assuming the distance between pinhole and holographic plane is $f=1$ mm. In this situation, the width and length of each hogel or EI is $w = 2f \tan(\theta_x/2) = 0.89$ mm and $h = 2f \tan(\theta_y/2) = 0.35$ mm. The geometric relationship of the hologram calculation using a 3D point cloud model with two layers is shown in Figure 2(a). The first layer contains two Chinese characters “北航”, which has a distance of 10 mm while the second layer includes two Chinese characters “全息” with 20 mm from the holographic plane H. The two layer Chinese characters are shifted in the vertical direction to guarantee not to overlap when they are viewed from the front view for simplicity. The 3D model has a size of 64 mm \times 64 mm \times 10 mm (W \times H \times D) with 984K object points. The front view of the model is shown in Figure 2(b).

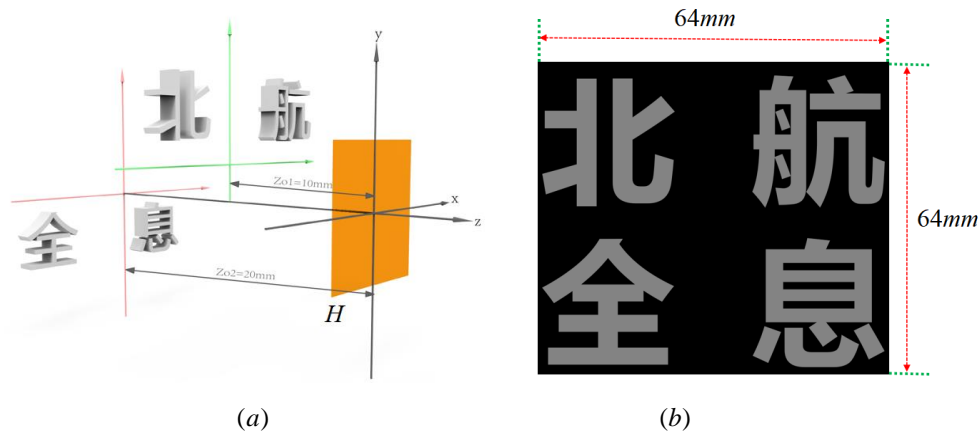


Figure 2. The geometric relationship for hologram calculation: (a) The side view of the holographic plane H and 3D model; (b) The front view of the 3D model.

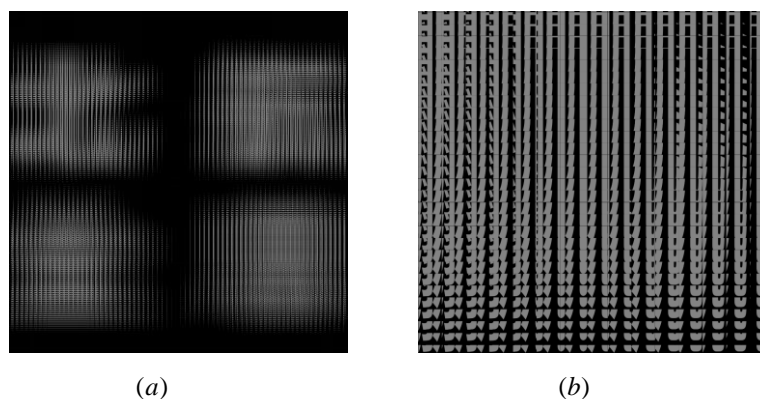
Table 1. Parameters for hologram calculation.

Parameters	Values
Number of points in the 3D model	984K
Size of hologram	63.6 mm × 63.6 mm
Resolution of hologram	200K × 200K
Pixel pitch of hologram	0.318 μm
Resolution of hogel	2800 × 1108 pixels
Wavelength	632 nm
Size of EI	0.89 mm × 0.35 mm
Pixel pitch of EI	4 μm
Resolution of EI	222 × 88 pixels
Number of EIs	71 × 181

In the rendering of the EIs, the sampling intervals for both x and y directions are set as 4 μm and the resolution of each EI is 222 × 88 pixels. The parameters for hologram calculation are summarized in Table I. In the proposed method, the size of EI is the same as the size of hogel, but the sampling intervals are different. After we get an EI from the 3D model, this EI is firstly interpolated to a new EI with the same resolution as the hogel. The interpolated EI is used for hologram calculation according to Eq. (5).

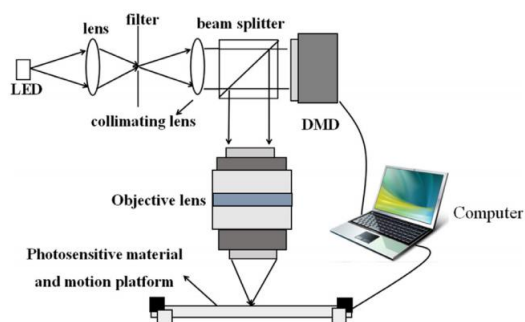
Figure 3(a) shows the rendered light field image, which contains all EIs rendered from the 3D model. Figure 3(b) is a partial enlarged light field image. The light field image almost has a resolution of 16K × 16K, which is higher than the resolution of current display panels. The high-resolution light field image and high-resolution hologram guarantee high imaging quality and large FOV of reconstructed 3D image.

Because of the independent property of calculation for each hogel in the proposed method, "parfor" in Matlab is used for parallel acceleration. The MATLAB 2015b with a laptop (i7-9750HQ CPU, 16G RAM and 1024G SSD) is used for hologram calculation. Six CPU cores participate in the hologram calculation. The computational time is about 8 minutes for calculation of this hologram including the time used for the EIs rendering. The hologram is printed with our home-made holographic printer from Institute of Information Optics, Zhejiang Normal University about 4.5 hours.



136
137
138

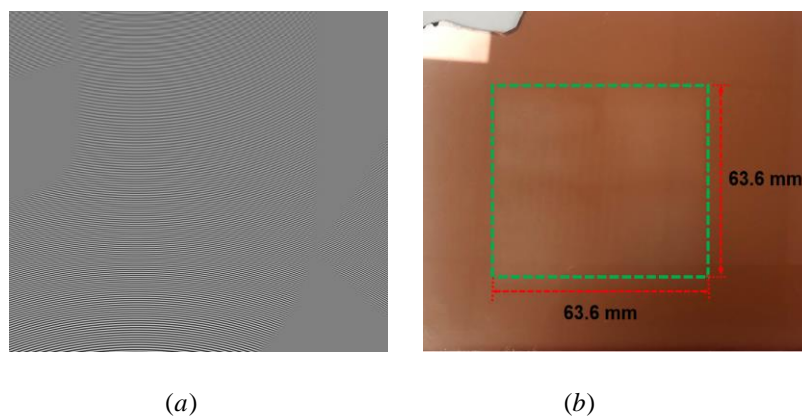
Figure 3. The rendered light field image: (a) Light field image; (b) Partial enlarged part of (a).



139
140

Figure 4. The diagram of holographic printer.

141 The overall diagram of the holographic printer is shown in Figure 4. The light from the LED is
142 filtered and collimated to illuminate the digital micro mirror (DMD) with a resolution of 1024×768
143 pixels. A small portion of the calculated hologram with resolution of 600×600 pixels is first zeros
144 padded to the same resolution as the DMD and then loaded into the DMD for display. The
145 modulated light from DMD is imaged on the photosensitive material through the objective lens and
146 this small portion hologram is printed. Controlled by computer, the motion platform is moved to the
147 next position for printing the next hologram section. With this holographic printer, the maximum
148 size of $200 \text{ mm} \times 200 \text{ mm}$ hologram with pixel pitch of $0.318 \mu\text{m}$ can be printed on photoresist plate.
149 The partial calculated hologram and the printed hologram are shown in Figures 5(a) and 5(b),
150 respectively.

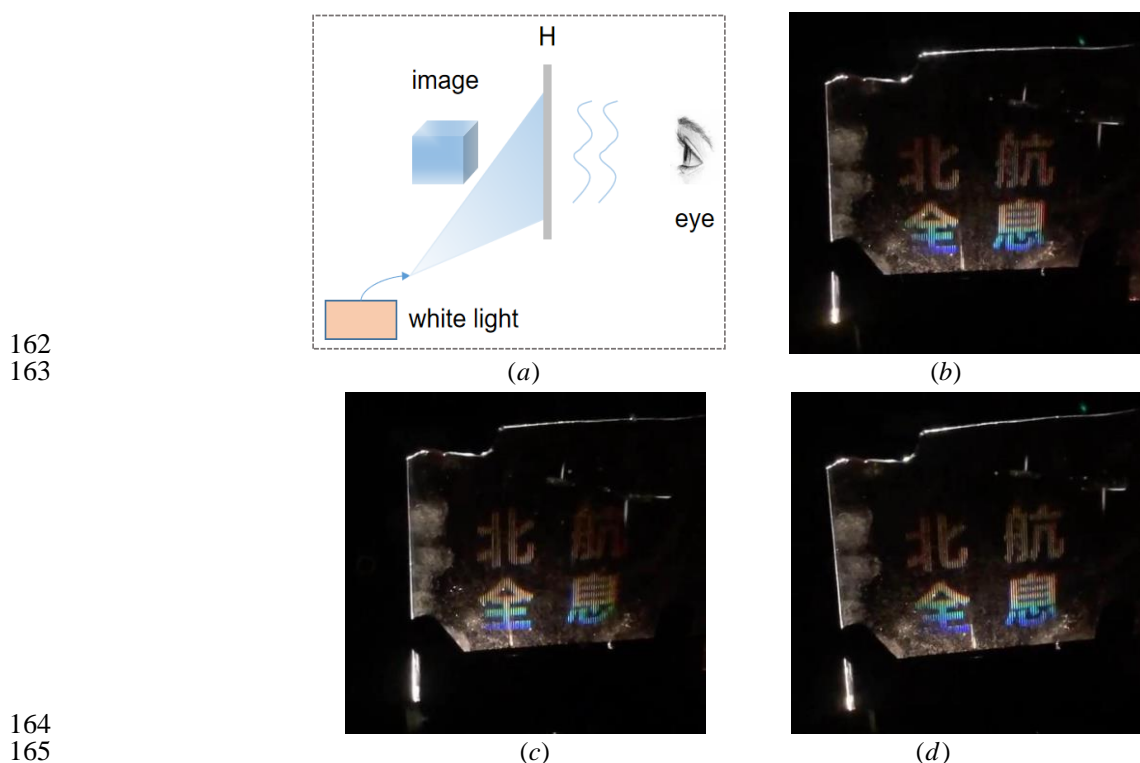


151
152
153

Figure 5. Hologram for 3D display: (a) Partial calculated hologram; (b) Printed hologram.

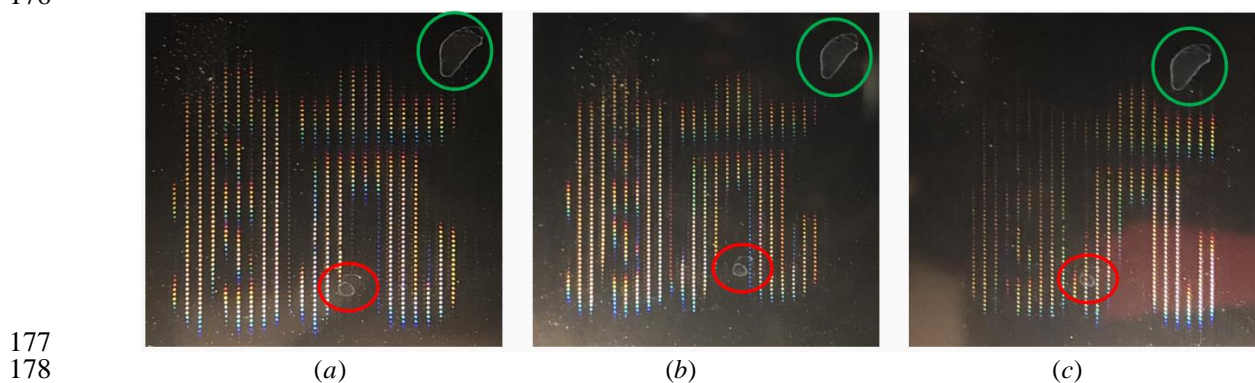
154 In the reconstruction, a halogen lamp available in our lab is used as illumination source. The
155 reconstruction of the hologram is demonstrated in Figure 6(a). The white light is coupled into the
156 fiber and a divergent light from the fiber head illuminates the hologram H with a proper incline
157 angle in the y direction. The diffracted light propagates into the human eye for watching the

158 reconstructed 3D image. Real image in front of the hologram plane or virtual image behind the
 159 hologram plane can be watched by selecting a proper illumination angle. Figures 6(b)-6(d) show
 160 three reconstructed images from three different viewing angles. And the supplementary video I
 161 shows the reconstruction from different viewpoints.



164
165
166 **Figure 6.** (a) The diagram of optical setup for reconstruction; (b)-(d) Different views of
 167 reconstructed 3D image. The supplementary video I shows the reconstruction from
 168 different viewpoints.

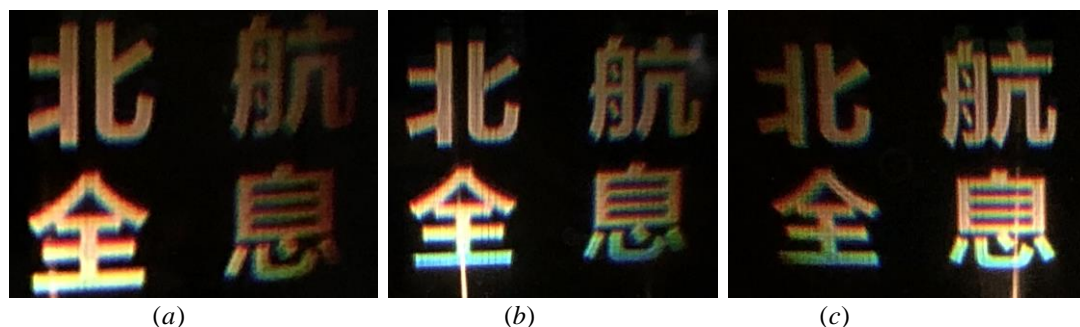
169 From the optical reconstruction, the parallax is smooth and the FOV is large. The brightness is a
 170 little difference due to the uneven incline illumination on this large area hologram. Figure 7 shows
 171 three images captured by our camera focusing on part of the holographic plane with different
 172 viewing angles. The two speckles in the red and green circles on the holographic plane are used as
 173 reference positions. From the results we can know that different perspective light coming from
 174 different position of the holographic plane, which is the core point of our method to encode the
 175 propagation of each pixel in EI to different angle with divergent sphere wave phase factor.
 176



179 **Figure 7.** (a)-(c) Three different images captured by the camera focused on the holographic plane.

180 In order to improve the quality of the displayed result, the second experiment is designed and
 181 carried out using the same model as the first experiment but with different parameters. In the second
 182 experiment, the distance between the pinhole array and holographic plane is $f = 0.25$ mm. In this

183 situation, each hogel has a resolution of 700×277 pixels corresponding to the physic size of 0.22 mm
184 $\times 0.09 \text{ mm}$. The sampling pitch in each EI is set as $1 \mu\text{m}$ and the resolution of each EI is 222×88 pixels,
185 which is the same as in the first experiment. The number of EIs is 287×725 . The resolution of full
186 light field image is about $63.7\text{K} \times 63.7\text{K}$ in this experiment. Other parameters are all the same as the
187 parameters of the first experiment. The calculation time of this hologram is approximate 37 minutes.
188 Figure 8 shows the three reconstructed images. And the supplementary video II shows the 3D
189 reconstruction from different viewing angles.



190
191
192
193

Figure 8. (a)-(c) Three reconstructed images from different viewpoints.
The supplementary video II shows the reconstruction from different viewpoints.

194 4. Discussion

195 To encode the high-resolution light field image into a high-resolution hologram has two
196 important advantages: displaying of 3D image with higher resolution and the dramatically
197 decreased calculation time of high-resolution hologram. In our proposed method, a pinhole array
198 behind the holographic plane is used for EIs rendering and a divergent sphere wave is used as the
199 phase information for each EI. However, the pinhole array can also be set in front of holographic
200 plane and convergent sphere wave is used as phase information.

201 In the calculation, converting each EI to the complex amplitude information on each hogel
202 plane using FFT is not needed in the proposed method. And the phase factor of divergent sphere
203 wave is the same for all hogels, which means the phase factor is only needed to be calculated one
204 time and reused for each hogel calculation. This direct encoding method can greatly reduce the
205 computational time of high-resolution hologram.

206 In the encoding process of hologram, plane wave is used as reference wave for simplicity.
207 Actually, a divergent sphere wave is more practical because the white light we used or a white light
208 LED for illumination of the hologram is approximately a divergent wave. The reason why a white
209 light can be used to reconstruct the hologram is that the distance between the reconstructed image
210 and the holographic plane is near, similar to the case of the image holography, the color dispersion
211 due to the white light illumination does not have a large influence on the reproduced 3D image. It
212 should be noted that to display the hologram with laser as illumination is still possible with a higher
213 resolution of reconstructed 3D image but speckle noise will exist.

214 we demonstrate two experiments for 3D display with different hogel size and sampling pitch.
215 From the results, we can conclude that the calculation time is associated with the number of object
216 points in the 3D model and EIs as well as the sampling interval in each EI. Well-designed parameters
217 will guarantee high quality reconstructed image with a relative short computational time. The
218 parallel computing using a GPU (graphics processing unit) is still possible for reduction of
219 computational time further.

220 The displayed results with white light as illumination is a grayscale 3D display. However, the

221 concept of full color rainbow holography [9,12] can also be applied to our method for full color 3D
222 display at the cost of losing vertical parallax.

223 5. Conclusion

224 In this study, a simple and fast method for full parallax high-resolution holographic 3D display
225 is demonstrated without using FFT. The encoding of the high-resolution light field image with
226 holographic method to speed up the calculation is the essence of our method. A high-resolution
227 hologram with 4 billion pixels is calculated only within 8 minutes and the optical 3D reconstruction
228 is effectively approved by experiments. The proposed method has possibility used for static 3D
229 advertising and holographic packaging.

230 **Author Contributions:** X. Y. wrote the program for hologram calculation and completed the relevant
231 experiments; H. Z. and F. X. rendered the light field images and printed the hologram; H. Z. helped to discuss
232 the research and modified the document; K. H. helped to prepare data for printing; Y. L. and Q.-H. W. led the
233 project and provided supports.

234 **Funding:** This research was funded by National Key R&D Program of China, under Grant No. 2017YFB1002900
235 and by National Natural Science Foundation of China under Grant No. 61927809.

236 **Conflicts of Interest:** The authors declare no conflict of interest.

237 References

- 238 1. F. Yaras, H. Kang, and L. Onural. State of the art in holographic display: A survey. *J. Disp Technol.*, **2010**,
239 6(10), 443-454.
- 240 2. K. Matsushima, Y. Arima, and S. Nakahara. Digitized holography: modern holography for 3D imaging of
241 virtual and real objects. *Appl. Opt.*, **2011**, 50(34), H287-H284.
- 242 3. X. Yang, H. Zhang, and Q. W. A fast-computer-generated holographic method for VR and AR near-eye 3D
243 display. *Appl. Sci.*, **2019**, 9, 4164: 1-11.
- 244 4. S. Lin, D. Wang, Q. Wang, E. Kim. Full-color holographic 3D display system using off-axis
245 color-multiplexed-hologram on single SLM. *Opt. Laser Eng.*, **2020**, 126, 105895:1-9.
- 246 5. A. Maimone, A. Georgiou, and J. Kollin. Holographic near-eye displays for virtual and augmented reality.
247 *ACM Trans. Graph.*, **2017**, 36, 8501-8516.
- 248 6. X. Li, J. Liu, T. Zhao, and Y. Wang. Color dynamic holographic display with wide viewing angle by
249 improved complex amplitude modulation. *Opt. Express*, **2018**, 26, 2349-2358.
- 250 7. H. Gao, F. Xu, J. Liu, Z. Dai, W. Zhou, S. Li, Y. Yu, and H. Zheng. Holographic three-dimensional virtual
251 reality and augmented reality display based on 4K-spatial light modulators. *Appl. Sci.*, **2019**, 9, 1128:1-9.
- 252 8. S. Lin, H. Cao, and E. Kim. Single SLM full-color holographic three-dimensional video display based on
253 image and frequency-shift multiplexing. *Opt. Express*, **2019**, 27, 15926-15942.
- 254 9. Y. Shi, H. Wang, Y. Li, H. Jin, and L. Ma. Practical method for color computer generated rainbow
255 holograms of real-existing objects. *Appl. Opt.*, **2009**, 48, 4219-4226.
- 256 10. X. Yang, H. Wang, Y. Li, F. Xu, H. Zhang and J. Zhang. Large scale and high resolution
257 computer-generated synthetic color rainbow hologram. *J. Opt.*, **2019**, 21, 025601: 1-10.
- 258 11. X. Yang, H. Wang, Y. Li, F. Xu, H. Zhang, J. Zhang, and Q. Yan. Computer generated full-parallax
259 synthetic hologram based on frequency mosaic. *Opt. Commun.*, **2019**, 430, 24-30.
- 260 12. T. Yamaguichi, and H. Yoshikawa. High resolution computer generated rainbow hologram. *Appl. Sci.*,
261 **2018**, 8, 1955:1-11.
- 262 13. O. Kunieda, and K. Matsushima. High-quality full-parallax full-color three-dimensional image
263 reconstructed by stacking large-scale computer-generated volume holograms. *Appl. Opt.*, **2019**, 58,
264 G104-G111.

- 265 14. Y. Yamamoto, H. Nakayama, N. Takada, T. Nishitsuji, T. Sugie, T. Kakue, T. Shimobaba, and T. Ito.
266 Large-scale electroholography by HORN-8 from a point-cloud model with 400,000 points. *Opt. Express*,
267 **2018**, 26, 34259-34265.
- 268 15. P. Su, W. Cao, J. Ma, B. Cheng, X. Liang, L. Cao, and G. Jin. Fast computer-generated hologram generation
269 method for three-dimensional point cloud model. *J. Display Technol.*, **2016**, 12, 1688-1694.
- 270 16. D. Arai, T. Shimobaba, K. Murano, Y. Endo, R. Hirayama, D. Hiyama, T. Kakue, and T. Ito. Acceleration of
271 computer-generated holograms using tilted wavefront recording plane method. *Opt. Express*, **2015**, 23,
272 1740-1747.
- 273 17. J. Liu and H. Liao. Fast occlusion processing for a polygon-based computer-generated hologram using the
274 slice-by-slice silhouette method. *Appl. Opt.*, **2018**, 57, A215-A221.
- 275 18. D. Abookasis and J. Rosen. Three types of computer-generated hologram synthesized from multiple
276 angular viewpoints of a three-dimensional scene. *Appl. Opt.*, **2006**, 45, 6533-6538.
- 277 19. H. Zhang, Y. Zhao, L. Cao, and G. Jin. Fully computed holographic stereogram based algorithm for
278 computer-generated holograms with accurate depth cues. *Opt. Express*, **2015**, 23, 3901-3913.
- 279 20. D. Blinder, and T. Shimobaba. Efficient algorithms for the accurate propagation of extreme-resolution
280 holograms. *Opt. Express*, **2019**, 27, 29905-29915.
- 281 21. H. Zhang, H. Deng, J. Li, M. He, D. Li, and Q. H. Wang. Integral imaging-based 2D/3D convertible
282 display system by using holographic optical element and polymer dispersed liquid crystal. *Opt. Lett.*,
283 **2019**, 44, 387-390.
- 284 22. Y. Zhang, Y. Fu, H. Wang, H. Li, S. Pan, and Y. Du. High resolution integral imaging display by using a
285 microstructure array. *J. Opt. Technol.*, **2019**, 86, 100-104.
- 286 23. L. Ai, H. Cao, H. Sun, and X. Shi. Performance enhancement of integral imaging based Fresnel hologram
287 capturing by the intermediate view reconstruction. *Opt. Express*, **2019**, 27, 31942-31955.
- 288 24. X. Zhang, G. Lv, Z. Wang, Z. Hu, S. Ding, and Q. Feng. Resolution-enhanced holographic stereogram
289 based on integral imaging using an intermediate-view synthesis technique. *Opt. Commun.*, **2020**, 457,
290 124656:1-6.